



1                   **Design of Wide Particle Size Range Aerodynamic Inlet System**  
2                   **with New Pre-focus Structure**

3   **Junhong Huang**<sup>1</sup>, **Lei Li**<sup>2,3</sup>, **Xue Li**<sup>2,3</sup>, **Zhengxu Huang**<sup>2,3</sup> and **Zhi Cheng**<sup>4</sup>

4   <sup>1</sup>Guangdong MS institute of scientific instrument innovation, Guangzhou, 510632,  
5   China

6   <sup>2</sup>Institute of Mass Spectrometry and Atmospheric Environment, Jinan University,  
7   Guangzhou, 510632, China

8   <sup>3</sup>Guangdong Provincial Engineering Research Center for On-Line Source  
9   Apportionment System of Air Pollution, Guangzhou, 510632, China

10   <sup>4</sup>Institute of Systems Engineering, Academy of Military Sciences, Tianjin, 300161,  
11   China

12

13   **Correspondence:** Lei Li (lileishdx@163.com)

14

15   **Abstract:** A new aerodynamic lens injection system has been designed for wide particle size  
16   range, which adds virtual impact and pre-focus structure on the basis of traditional PM2.5 lenses.  
17   The system has a small volume and successfully improves the focusing ability of traditional  
18   PM2.5 lens systems to 100 nm-10 μm. The structure of the new pre-focus hole solves the problem  
19   of affecting the transmission and focusing of large particles, effectively reducing the beam width  
20   and dispersion angle of particles entering the virtual impactor, significantly improving the  
21   focusing effect of large particles, and enhancing the transmission efficiency of large particles. It  
22   can also effectively focus particles without significantly accelerating particles, avoiding the  
23   structural size of the buffer chamber being too large. Numerical simulation shows that the new  
24   injection system can transmit particles with 100% efficiency in the range of 0.2-4 μm particles,  
25   and can achieve the transmission of 1-9 μm particles with an efficiency higher than 90%. The  
26   standard microsphere experiment verified the good consistency between the performance of the  
27   injection system and the simulation results. In the testing of standard Arizona dust, the wide-range  
28   particle size distribution obtained by the new injection system is highly consistent with APS 3321.  
29   The new injection system combines a new pre-focus structure, a smaller buffer chamber, a five-  
30   stage lens, and the whole injection system volume that is up to 90% smaller than previous self-  
31   made wide-range lens designs. At the same time, it has ultra-high transmission efficiency,  
32   demonstrating the potential for miniaturization of single particle aerosol mass spectrometer in  
33   detecting particles with a wide particle size range.

34   **Keywords:** Aerosol particles; Aerodynamic lens; Beam width; Transmission efficiency;  
35   Numerical simulation



36

## 37 **1 Introduction**

38 As a key component of aerosol mass spectrometry, the particle beam generator is used to  
39 focus the injected particles, and the focusing ability of the particle beam determines the detection  
40 sensitivity of the aerosol mass spectrometer. As a common particle beam focusing device,  
41 aerodynamic lenses (Liu et al., 1995; Murphy et al., 2006; Zelenyuk et al., 2015; Clemen et al.,  
42 2020) utilize the inertia difference between particles and fluids to focus particles and are widely  
43 used in different aerosol mass spectrometry (Peck et al., 2016). In addition to its application in  
44 aerosol mass spectrometry, aerodynamic lens systems have also been applied in many analytical  
45 equipment. Researchers use aerodynamic lenses to introduce aerosol particles into pulsed X-ray  
46 beams and determine the particle composition using diffraction patterns and ion fragments  
47 generated when the X-ray pulse meets the particle (Loh et al., 2012). Aerodynamic lenses can also  
48 be used in the mass spectrometry of nano-mechanical resonators. They can achieve efficient  
49 transmission and focusing of large analytes without the need for ionization, significantly  
50 improving the performance of nano-mechanical mass spectrometers (Dominguez-Medina et al.,  
51 2018).

52 Although aerodynamic lenses have significant transmission effect on particles, the particle  
53 size range designed by most current aerodynamic lens is mainly within an order of magnitude, and  
54 the size range that can be focused is mainly below 3  $\mu\text{m}$  (Ferguson et al., 2004; Srivastava et al.,  
55 2005; Tobias et al., 2006). Such as the 25-250 nm of Liu et al. (1995), the 100-900 nm and the  
56 340-4000 nm of Schreiner et al. (1998; 1999), the 60-600 nm of Zhang et al. (2004), and the 125-  
57 600 nm of Zelenyuk et al. (2015). The particle size of aerosols in the atmosphere ranges from sub-  
58 nanometer to millimeter level, and focusing sample injection of particles with a wide particle size  
59 range is crucial for improving the analytical ability of aerosol mass spectrometry, such as the  
60 analysis of biological aerosols, dust, single cells.

61 Researchers have been working to expand the transmission range of particles by aerodynamic  
62 lenses. Research has shown that the focusing performance of aerodynamic lenses for small  
63 particles below 50 nm is limited by Brownian motion, while focusing on large particles is mainly  
64 affected by the larger inertia of particles (Wang et al., 2005; Wang and McMurry, 2006). At present,  
65 most of the reported aerodynamic lenses have low efficiency in transmitting large particle size  
66 (Cahill et al., 2014; Deng et al., 2008; Williams et al., 2013; Wu et al., 2009), so the key to  
67 achieving simultaneous transmission with a wide particle size range is to improve the focusing  
68 performance of large particles. The most direct method is to increase the stage number of lenses.  
69 For example, Lee et al. (2013) designed a seven-stage lens for particle detection in the range of 30  
70 nm to 10  $\mu\text{m}$ , but this study does not consider the impact of critical holes on the transmission loss  
71 of large particles and it is not applied in practice. Cahill et al. (2014) designed a high-pressure lens,  
72 and used a very long buffer chamber combined with a seven-stage lens to transmit 4-10  $\mu\text{m}$



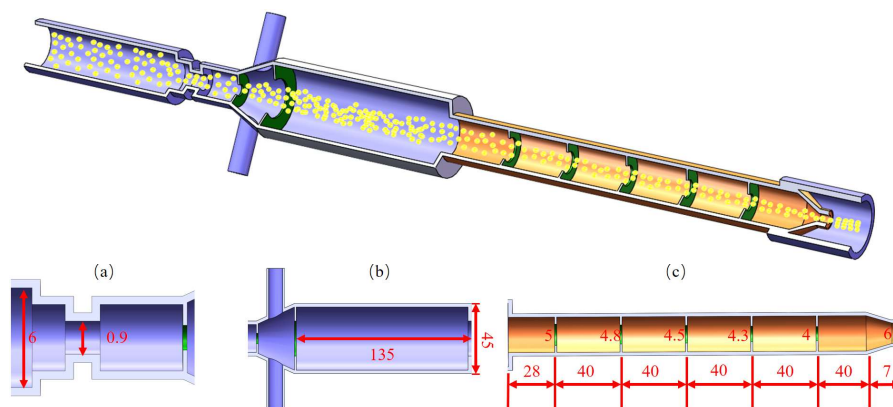
73 particles. However, experiments show that the transmission efficiency of 4  $\mu\text{m}$  and 9  $\mu\text{m}$  particles  
74 is only 20%, and the overall size of the lens system is relatively large. Increasing the stage number  
75 of lens is obviously beneficial for the transmission of wide-range particle size, but it can also lead  
76 to excessive volume of the injection system and increased assembly difficulty, as Liu et al. (2007)  
77 mentioned in the report that the beam focusing effect will decrease with the decrease in assembly  
78 accuracy of the aerodynamic lens system.

79 Hari et al. (2007) added a virtual impactor behind the critical hole, and their study shows that  
80 using the virtual impactor structure can reduce the cross trajectory phenomenon of large particles,  
81 which is beneficial for improving the transmission performance of large particles in the injection  
82 system. Chen et al. (2007) investigated the effect of the front and rear structure of critical hole on  
83 particle loss through numerical simulation and experimental verification, and optimized the  
84 structure to enhance the transmission efficiency of particles with 50nm and below, but the  
85 transmission range is not significantly extended. Liu et al. (2007) unified the inner diameter of the  
86 downstream pipeline of the critical hole to reduce the wall impingement loss of particles. Hwang  
87 et al. (2015) proposed a new type of critical hole, which can effectively reduce the incident angle  
88 of large particle beams through a converging-diverging structure design and achieve particle  
89 transmission in the range of 30 nm to 10  $\mu\text{m}$ . However, the critical hole is difficult to fabricate due  
90 to the limitation of processing technology and has not been applied in practice. The above studies  
91 indicate that the large particles in the aerodynamic lens system loss on the surface of the critical  
92 hole. Du et al. (2023) proposed a pre-focus design for the first time to address the shortcomings of  
93 loss caused by large particles hitting the surface of the critical hole. A two-stage lens is added at  
94 the front of the critical hole, so that large particles could be focused on the axis to a greater extent  
95 before entering the critical hole. This design greatly reduces the beam incident angle of large  
96 particles in front of the critical hole, thereby reducing the impact loss of large particles on the  
97 surface of the critical hole. Combined with the seven-stage lens, efficient transmission of 62 nm-  
98 13  $\mu\text{m}$  particles is achieved. However, due to the acceleration of particles after passing through the  
99 pre-focus lens, their downstream divergence angle after leaving the critical hole is large. Therefore,  
100 it is necessary to match a buffer chamber with a diameter of 250 mm to achieve efficient  
101 transmission of particles with a wide particle size range mentioned above. This design results in a  
102 very large overall size of the injection system, which is not conducive to the miniaturization of  
103 mass spectrometer.

104 This paper introduces a newly designed and manufactured small-volume pre-focus wide-  
105 range aerodynamic lens injection system (PFW-ALens) for transporting particles with diameters  
106 ranging from 100 nm to 10  $\mu\text{m}$ . The key components of the injection system include a novel low-  
107 pressure loss pre-focus hole structure, a small buffer chamber and a five-stage aerodynamic lens  
108 group. Computational fluid dynamics software is used to model the transmission performance  
109 from the sampling inlet to the nozzle, and it is verified by experiments. Numerical simulation  
110 shows that the transmission efficiency of particles in the range of 100 nm-9  $\mu\text{m}$  is higher than 90%.



111 In experimental verification, the transmission efficiency of particles in the range of 100 nm-5  $\mu\text{m}$   
 112 is above 90%, and the transmission efficiency of particles in the range of 9  $\mu\text{m}$  and below is more  
 113 than 50%. This lens system has great potential for application in bioaerosol analysis, sand and dust  
 114 analysis, and miniaturization of mass spectrometer.



115  
 116 Fig. 1 Structural design of the injection system. Locally displayed are the pre-focus hole (a),  
 117 buffer chamber (b), and aerodynamic lens system (c).

## 118 2 Numerical simulation and experimental design

### 119 2.1 Physical models

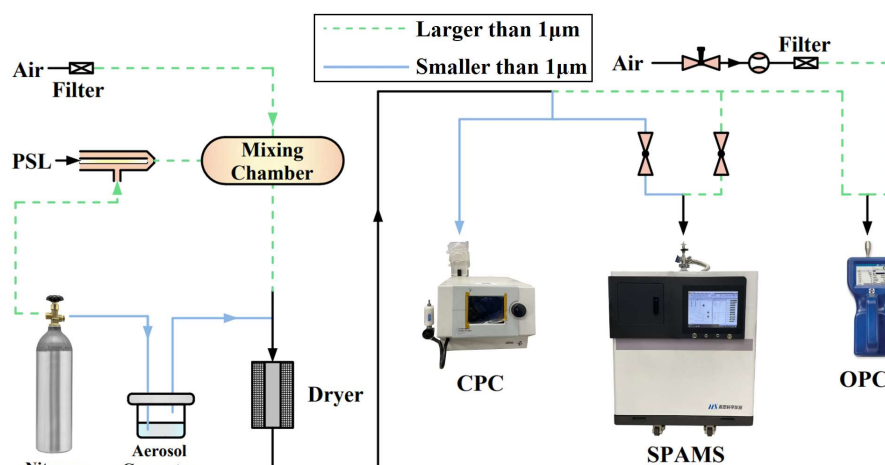
120 Fig. 1 shows the structure of the injection system, which consists of four modules, namely the  
 121 pre-focus hole, the separation cone, the buffer chamber, and the aerodynamic five-stage lens group.  
 122 Fig. 1(a ~ c) respectively represent the critical dimensions of each component. Aerosol particles  
 123 approach the centerline through pre-focus holes, and a separation cone with diameter of 1 mm and  
 124 angle of  $15^\circ$  is set 1.6 mm downstream of the critical hole. The excess air between the critical hole  
 125 and the separation cone is extracted by a side pump to achieve the concentration effect of aerosol  
 126 particles, which then enter the buffer chamber. The particles accelerated through the critical hole  
 127 gradually decelerate in the buffer chamber, and then are driven by the airflow into the  
 128 aerodynamic lens system. The aerodynamic lens system consists of five apertures with diameters  
 129 of 5 mm, 4.8 mm, 4.5 mm, 4.3 mm and 4 mm, respectively, and an accelerating nozzle with a  
 130 diameter of 3 mm. The length from the inlet of the buffer chamber to the outlet of the acceleration  
 131 nozzle is 370 mm, and the distance between the same components in the injection system designed  
 132 by Du et al. is 570 mm. The aerodynamic lens system consisting of different diameters of  
 133 apertures can effectively focus aerosol particles within a certain range onto the axis of the lens.  
 134 Finally, aerosol particles are further accelerated by the action of the accelerating nozzle and enter  
 135 the subsequent diameter measurement system.

### 136 2.2 Numerical model



137 Ansys-Meshing is used to generate the mesh, and Fluent software is used to calculate the  
 138 flow of gas and particle coupling between the sampling inlet and the accelerating nozzle. The  
 139 pressure at the sampling inlet is set to 101325 Pa, the outlet pressure of the virtual impactor is set  
 140 to 600 Pa, the buffer chamber and the aerodynamic lens group used are both set to operate in an  
 141 environment below 300 Pa, and the pressure at the outlet of the accelerating nozzle is 0.1 Pa. The  
 142 parameter settings are consistent with the study of Zhang et al. (2002). In addition, the Viscous  
 143 model used in the simulation is laminar flow model. The discrete format of the flow equation is  
 144 second-order upwind. The motion of aerosol particles will use the User Define Function (UDF) to  
 145 load the particle resistance model and the Brownian force model. By setting the number, diameter,  
 146 and release position of particles in the DPM model, the trajectory and velocity of particles can be  
 147 obtained through cloud images.

148 **2.3 Experimental exploration**



149  
150 Fig. 2 Gas path connection in experiment

151 Standard polystyrene latex spheres (PSL, Thermo Fisher Scientific) ranging from 100 nm to  
 152 10 μm are used to characterize the focusing ability of aerodynamic lens system. The operation for  
 153 generating and counting aerosols larger than 1 μm is as follows. First, the PSL solution is diluted  
 154 with pure water, and then nitrogen is used as carrier gas to atomize the PSL solution using ICPMS  
 155 atomizer before passing it into the mixing chamber, where the injection rates of PSL solution and  
 156 nitrogen are 10 μL/min and 0.2 L/min, respectively. The excess moisture in the atomized aerosol  
 157 particles is removed by heating the mixing chamber and introducing a drying tube, and then the  
 158 aerosol particles are introduced into the optical particle counter (OPC, TSI, Model 9306) and  
 159 SPAMS respectively through a three-way tube for counting. For particles below 1 μm, aerosol  
 160 generator (TSI, Model 9302) is used to generate aerosols and condensed particle counter (CPC,  
 161 TSI, Model 3775) is used for counting. The specific gas path connection is shown in Fig. 2, where  
 162 the blue solid line is the test pipeline connection scheme for the transmission efficiency of  
 5 / 16



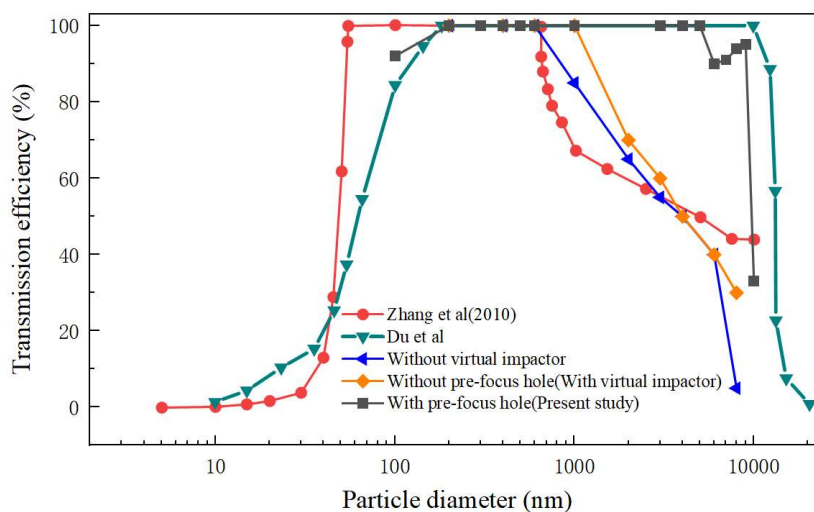
163 particles below 1  $\mu\text{m}$ , and the green dotted line represents the test pipeline connection scheme for  
164 the transmission efficiency of particles above 1  $\mu\text{m}$ .

165 The single particle mass spectrometer used in this study is similar to HP-SPAMS (Du et al.,  
166 2024), but its optical system has been improved. The first diameter measuring laser is designed as  
167 a beam splitting optical structure similar to APS3321, and the dual beam can measure the  
168 aerodynamic diameter of particles. Photomultiplier tube PMT is used to detect the number of  
169 particles passing through the laser. In the experiment, we regard the total number of PMT  
170 detections obtained per unit time as the total number of particles entering SPAMS. For particles  
171 larger than 1  $\mu\text{m}$ , the particle count of the corresponding size in OPC is taken as the total number  
172 of particles of that size, and the transmission efficiency of that particle size is the ratio of the total  
173 number of particles entering OPC and SPAMS, respectively. For particles below 1  $\mu\text{m}$ , the  
174 transmission efficiency is the ratio of the particle concentration recorded by PMT to the particle  
175 concentration recorded by CPC.

## 176 **3 Results and discussions**

### 177 **3.1 Aerodynamic lens with virtual impact**

178 The basic model of aerodynamic lenses is consistent with that of Zhang et al. (2004), as  
179 shown in Fig. 3. Simulation results of Zhang et al. show that the focusing range of the lens of this  
180 size is mainly between 50 nm and 3  $\mu\text{m}$ , and the transmission efficiency of 1.5  $\mu\text{m}$  is 50%. The  
181 initial condition of this simulation is to assume that particles are uniformly distributed from the  
182 buffer chamber to the front of the lens, but in fact, for large particles, the state of entering the lens  
183 is not the same. Many scholars (Canagaratna et al., 2007; Drewnick et al., 2009; Meinen et al.,  
184 2010; Docherty et al., 2013;) have used this lens system to carry out different studies, and added a  
185 buffer chamber and a virtual impactor structure as shown in Fig. 1(a) on the basis of this model.  
186 By comparing the particle transmission efficiency curves before and after adding a virtual  
187 impactor, it can be found that after the addition of the virtual impactor (orange diamond symbol  
188 line), the focusing ability of the injection system for particles larger than 1  $\mu\text{m}$  has increased to  
189 varying degrees, and the transmission efficiency of 7  $\mu\text{m}$  particles has increased from the original  
190 5% to 30%. Although the aerodynamic lens system with virtual impact structure has increased its  
191 ability to focus on large particles, this particle size range is still insufficient for the detection of  
192 large particle aerosols such as dust and organisms.



193

194

Fig. 3 Curves of particle focusing ability for different injection systems

195

### 3.2 Pre-focus injection system

196

197

198

199

200

201

202

203

204

205

206

207

208

209

210

211

212

213

214

215

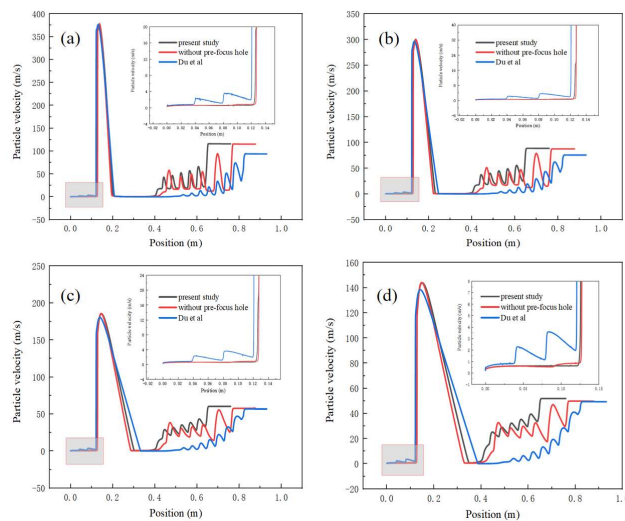
216

217

In response to the shortcomings mentioned in section 3.1 regarding the transmission range of particles and the low transmission efficiency of larger particles, Du et al. pointed out that an important reason for the loss of large particles is that particles hit the surface of the critical hole to form the wall impingement loss. They proposed a pre-focus injection technique, which involves placing a set of two-stage lenses in the injection tube in front of the critical hole. The lenses can focus the particles to the axis in advance, avoiding the wall impingement loss of particles. This structure can reduce the loss of 10  $\mu\text{m}$  particles from the original about 40% to 0. The curve in Fig. 3 shows that the seven-stage aerodynamic lens system with pre-focus structure designed by Du et al. can achieve efficient transmission in a wide particle size range of 0.18-10  $\mu\text{m}$ . Although the lens of Du et al. can achieve a wide range, the overall lens system still has shortcomings. The main problem is that the particle beam diverges greatly after passing through the critical hole and virtual impact hole, so a large buffer with a diameter of 250 mm and a height of 250 mm is needed to release particles in the full particle size range. Combined with the seven-stage aerodynamic lens, the overall size and volume of the lens system can reach a diameter of 278 mm and a height of 875 mm. This is mainly because the design of the pre-focus lens produces a pressure loss, and the particles are focused on the central axis while also obtaining a large acceleration, which probably increases the divergence of the particles entering the strong buffer. As shown in Fig. 4, it can be found that the pre-focus structure makes the particles of different sizes accelerated compared with other systems. It can be found in Fig. 5(b) that the dispersion angle of 5  $\mu\text{m}$  particles is also very large after leaving the critical hole, so a particularly large buffer chamber is needed to achieve particle collection and deceleration before entering the lens system to complete focusing. A large-size injection system is not only detrimental to the miniaturization of mass spectrometer, but also a



218 seven-stage lens system can also lead to the increase of assembly accuracy, and the consistency of  
219 the lens is difficult to ensure.

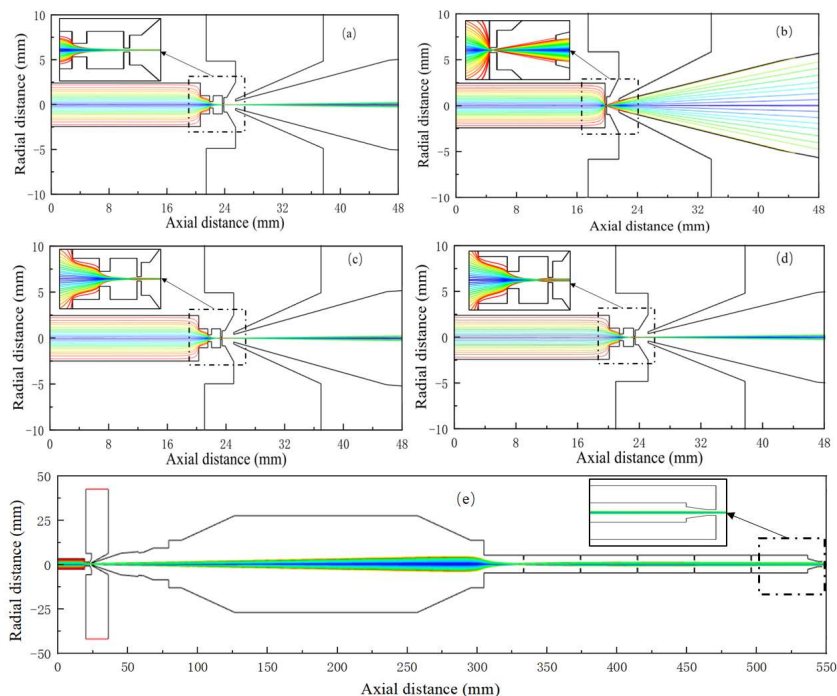


220

221 Fig. 4 Axial velocity of particles in different injection systems. (a) ~ (d) represent particles of 0.5

222

μm, 1 μm, 3 μm, and 5 μm, respectively



223

224 Fig. 5 Trajectories of large particles in different injection systems. (a) and (b) represent particle of

225 5 μm in the new and old systems, and (c) represents particle of 6 μm in the new system. (d) and (e)

226

represent local and global trajectory of 8 μm

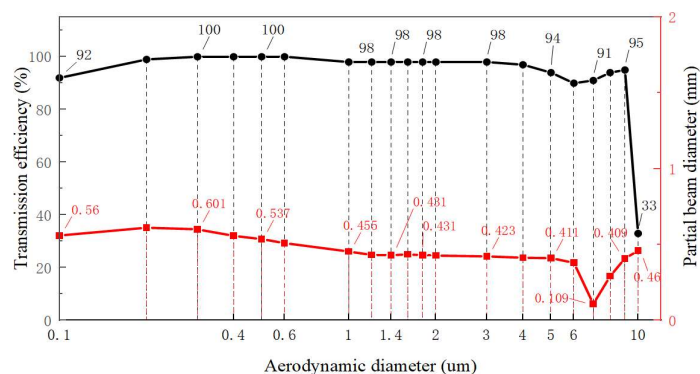




### 227 3.3 New design

228 In this study, a new single-stage pre-focus structure is designed, which is equivalent to the  
229 critical hole as a two-stage lens. The specific structural dimensions are shown in Fig. 1. In the  
230 previous text, the pre-focus structure of Du will lead to particle acceleration and large dispersion  
231 angle, which will directly affect the size of the buffer chamber design and the focusing ability of  
232 the lens group. Therefore, the pressure drop of the pre-focus structure and the dispersion angle of  
233 particles are required in the design process. As shown in Fig. 4, the velocity distribution of 0.5  $\mu\text{m}$ ,  
234 1  $\mu\text{m}$ , 3  $\mu\text{m}$ , and 5  $\mu\text{m}$  particles under three different systems is compared. It can be found that the  
235 acceleration effect of particles in the pre-focus structure of Du is obvious, while the acceleration  
236 effect of the new pre-focus structure on particles is almost the same as that without the pre-focus  
237 structure. This means that the pre-focus hole used by PFW-ALens achieves pre-focus of large  
238 particles without additional acceleration effect on particles, which is more conducive to reducing  
239 the degree of change in the subsequent injection system. This also provides a good foundation for  
240 optimizing the length of the lens system and reducing the number of lenses.

241 The beam divergence angle of particles after passing through the critical hole directly affects  
242 the design of the buffer chamber and the transmission efficiency of particles (Lee et al., 2013).  
243 The greater the divergence degree, the easier it is for the particles to collide with the pipeline wall  
244 and cause losses. Therefore, the divergence angle after the critical hole determines the  
245 transmission range and efficiency of particles, especially for large particles. Fig. 5 shows the  
246 advantages of the new pre-focus structure for the transmission of large particles. Fig. 5a and Fig.  
247 5b represent the transmission trajectories of 5  $\mu\text{m}$  particles in PFW-ALens and the injection  
248 system without pre-focus holes, respectively. It can be observed that the divergence of particles  
249 after passing through the critical hole is much greater in the structure without pre-focus, so it is  
250 necessary to adapt to a larger buffer chamber. Even the buffer chamber structure used by the pre-  
251 focus lens structure of Du et al. reaches 250 mm \* 250 mm. Fig. 5c and Fig. 5d show that even for  
252 larger particles of 6  $\mu\text{m}$  and 8  $\mu\text{m}$ , PFW-ALens can maintain a very small divergence angle. In fact,  
253 the structural size of the buffer chamber we used is 45 \* 135 mm, and the volume of the buffer  
254 chamber is reduced by more than 90% compared to the previous one.



255

Fig. 6 Transmission efficiency and particle beam width of new injection system

256

257

258

259

260

261

262

263

264

265

266

267

268

269

270

271

272

273

274

275

The overall transmission characteristics of the lens model are simulated, and the transmission efficiency is obtained by calculating the ratio of the number of particles at the sampling inlet and the outlet of the nozzle. The beam width is obtained by exporting the radial distribution coordinates of particles 110 mm downstream of the nozzle using Fluent software and then calculating its 90% quantile. It can be seen from Fig. 6 that the particle transmission range of PFW-ALens is greatly increased, maintaining a transmission efficiency of over 90% for particles in the range of 100 nm to 9 μm, until the transmission efficiency of 10 μm particles shows a cliff-like decline. At the same time, the simulation results show that the beam width can be kept below 0.6 mm throughout the whole particle size transmission range. In fact, the transmission efficiency of 10 μm particles can be further increased by improving the structure. Simulation results show that increasing the length of the buffer chamber can greatly improve the above efficiency, so the efficient transmission of 9 μm is not the upper limit of this system. In general, the particle focusing ability exhibited by PFW-ALens in the range of 10 μm is almost consistent with the focusing performance of Du et al. in the same detection range. It is worth noting that the lens model used in this study is a PM2.5 five-stage lens, while most of the wide-range lenses generally use the structure of seven-stage lenses. This shows that the pre-focus device used in this study can not only focus large particles more effectively, but also accomplish focusing with fewer lenses, thereby reducing the volume of the injection system. This is of great significance for the miniaturization of high-performance single particle mass spectrometer.

276

### 3.4 Validation and application

277

278

279

280

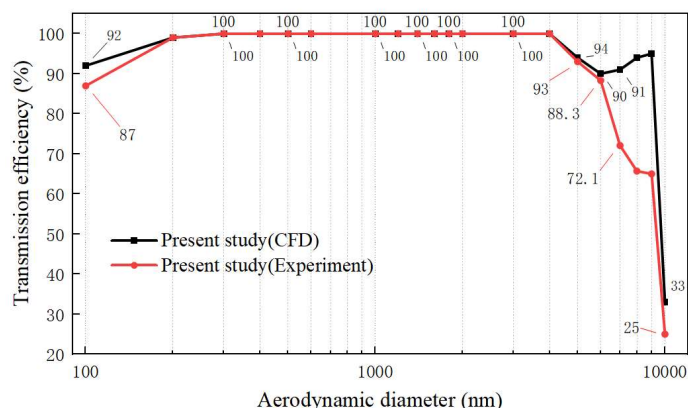
281

282

Fig. 7 compares the transmission efficiency of particles with different particle sizes in numerical simulation and experimental validation of PFW-ALens. It can be found that the experimental verification results are basically in good agreement with the numerical simulation in the whole particle size range. The actual test of the transmission efficiency of 200 nm - 6 μm particles can be maintained at more than 90%, and the actual test of 100 nm particles can also reach more than 87%. In fact, 100nm particles will also cause some measurement loss due to the



283 light scattering intensity. For particles with a particle size greater than 6  $\mu\text{m}$ , the testing effect  
 284 shows a significant decrease in efficiency, but 9  $\mu\text{m}$  particles can still remain above 65%. The  
 285 trend of 10  $\mu\text{m}$  particles is consistent with the simulation results, with a transmission efficiency of  
 286 only 25%. The decrease in efficiency of large particles may be attributed to inconsistent  
 287 transmission losses of particles between OPC and B-SPAMS.



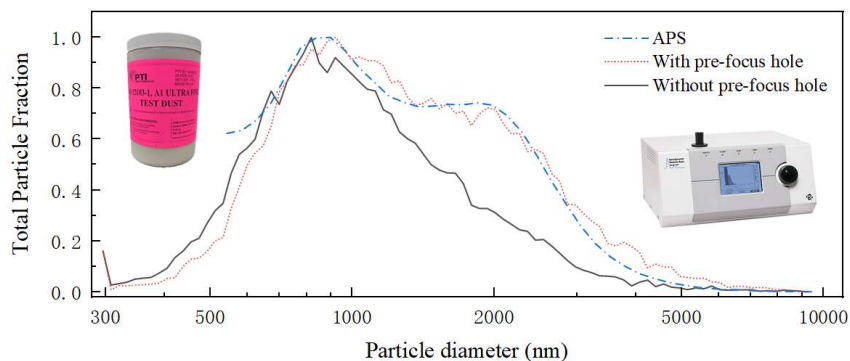
288

289

Fig. 7 Experimental verification of particle transmission

290

In order to characterize the analytical ability of PFW-ALens for large particles, the standard  
 291 ULTRAFINE TEST DUST from Arizona is selected as the test sample. Firstly, APS is used to  
 292 detect dust as a standard, and then PFW-ALens with pre-focus holes (red dotted line) and injection  
 293 systems without pre-focus holes (black solid line) are used for testing and comparison. The  
 294 specific particle size distribution is shown in Fig. 8, and the particle size distribution measured by  
 295 PFW-ALens is closer to that measured by APS. The above experiments not only prove that PFW-  
 296 ALens can more accurately detect the particle size distribution of dust compared to injection  
 297 systems without pre-focus holes, but also prove that PFW-ALens can achieve efficient  
 298 transmission of large particles, demonstrating the potential of new lens structure in detecting large  
 299 particle analysis.



300

301

Fig. 8 Particle size distribution of standard dust in different injection systems



## 302 **5 Conclusions**

303 In order to improve the transmission efficiency of large particles in the SPAMS injection  
304 system and reduce the volume of the injection system, this study developed an injection system  
305 PFW-ALens with the ability to focus large particles. This injection system adopts a new pre-focus  
306 structure, which can effectively reduce the size of buffer chamber and the number of lenses  
307 compared to the injection system with traditional pre-focus holes, while maintaining a low-loss  
308 transmission effect for particles with a larger particle size range. By adding a pre-focus structure,  
309 the focusing ability of the 2.5  $\mu\text{m}$  lens system is significantly improved to 10  $\mu\text{m}$ .

310 The numerical simulation results show that the newly designed injection system can achieve  
311 the focusing and transmission of particles with particle size ranging from 100 nm to 10  $\mu\text{m}$ .  
312 Among them, the beam width of large particles after leaving the separation cone is significantly  
313 reduced compared to existing injection systems, which has extremely high particle transmission  
314 efficiency. The results show that the transmission efficiency can be higher than 90% when the  
315 particle size is less than 9  $\mu\text{m}$ . Particles with a range of 200 nm-4  $\mu\text{m}$  have a transmission  
316 efficiency of 100%. The injection system designed in this paper is currently the one that achieves  
317 the widest particle size range and highest transmission efficiency in the same structural size. This  
318 design is beneficial for further reducing the structural size of the injection system and the number  
319 of aerodynamic lenses, which provides ideas and inspiration for the miniaturization of the mass  
320 spectrometer.

321

322

323 *Data availability.* These data can be publicly accessible in free.

324

325 *Author contributions.* LL and ZXH designed the study; JHH and XL performed the  
326 simulations and experiments; JHH, LL, XL, ZXH and ZC participated in data analysis  
327 and result discussion; JHH and LL wrote the paper with the input from all authors.

328

329 *Competing interests.* The authors declare that they have no conflict of interest.

330

331 *Financial support.* This research was funded by the National key research and  
332 development program for young scientists (2022YFF0705400) and the Fundamental  
333 Research Funds for the Central Universities (21623205) .

334

## 335 **References**

336 Cahill, J. F., Darlington, T. K., Wang, X., Mayer, J., Spencer, M. T., Holecek, J. C., Reed, B. E.,



- 337 and Prather, K. A.: Development of a High-Pressure Aerodynamic Lens for Focusing Large  
338 Particles (4–10  $\mu\text{m}$ ) into the Aerosol Time-of-Flight Mass Spectrometer, *Aerosol Science and*  
339 *Technology*, 48, 948-956, 10.1080/02786826.2014.947400, 2014.
- 340 Canagaratna, M. R., Jayne, J. T., Jimenez, J. L., Allan, J. D., Alfarra, M. R., Zhang, Q., Onasch, T.  
341 B., Drewnick, F., Coe, H., Middlebrook, A., Delia, A., Williams, L. R., Trimborn, A. M.,  
342 Northway, M. J., DeCarlo, P. F., Kolb, C. E., Davidovits, P., and Worsnop, D. R.: Chemical and  
343 microphysical characterization of ambient aerosols with the aerodyne aerosol mass  
344 spectrometer, *Mass Spectrometry Reviews*, 26, 185-222, 10.1002/mas.20115, 2007.
- 345 Chen, S.-C., Tsai, C.-J., Wu, C.-H., Pui, D. Y. H., Onischuk, A. A., and Karasev, V. V.: Particle loss  
346 in a critical orifice, *Journal of Aerosol Science*, 38, 935-949, 10.1016/j.jaerosci.2007.06.010,  
347 2007.
- 348 Clemen, H.-C., Schneider, J., Klimach, T., Helleis, F., Köllner, F., Hünig, A., Rubach, F., Mertes,  
349 S., Wex, H., Stratmann, F., Welti, A., Kohl, R., Frank, F., and Borrmann, S.: Optimizing the  
350 detection, ablation, and ion extraction efficiency of a single-particle laser ablation mass  
351 spectrometer for application in environments with low aerosol particle concentrations,  
352 *Atmospheric Measurement Techniques*, 13, 5923-5953, 10.5194/amt-13-5923-2020, 2020.
- 353 Deng, R., Zhang, X., Smith, K. A., Wormhoudt, J., Lewis, D. K., and Freedman, A.: Focusing  
354 Particles with Diameters of 1 to 10 Microns into Beams at Atmospheric Pressure, *Aerosol*  
355 *Science and Technology*, 42, 899-915, 10.1080/02786820802360674, 2008.
- 356 Docherty, K. S., Jaoui, M., Corse, E., Jimenez, J. L., Offenberg, J. H., Lewandowski, M., and  
357 Kleindienst, T. E.: Collection Efficiency of the Aerosol Mass Spectrometer for Chamber-  
358 Generated Secondary Organic Aerosols, *Aerosol Science and Technology*, 47, 294-309,  
359 10.1080/02786826.2012.752572, 2013.
- 360 Dominguez-Medina, S., Fostner, S., Defoort, M., Sansa, M., Stark, A.-K., Halim, M. A., Vernhes,  
361 E., Gely, M., Jourdan, G., Alava, T., Boulanger, P., Masselon, C., and Hentz, S.: Neutral mass  
362 spectrometry of virus capsids above 100 megadaltons with nanomechanical resonators, *Science*,  
363 362, 918-922, 10.1126/science.aat6457, 2018.
- 364 Drewnick, F., Hings, S. S., Alfarra, M. R., Prevot, A. S. H., and Borrmann, S.: Aerosol  
365 quantification with the Aerodyne Aerosol Mass Spectrometer: detection limits and ionizer  
366 background effects, *Atmos. Meas. Tech.*, 2, 33-46, 10.5194/amt-2-33-2009, 2009.
- 367 Du, X., Zhuo, Z., Li, X., Li, X., Li, M., Yang, J., Zhou, Z., Gao, W., Huang, Z., and Li, L.: Design  
368 and Simulation of Aerosol Inlet System for Particulate Matter with a Wide Size Range,  
369 *Atmosphere*, 14, 10.3390/atmos14040664, 2023.
- 370 Du, X., Xie, Q., Huang, Q., Li, X., Yang, J., Hou, Z., Wang, J., Li, X., Zhou, Z., Huang, Z., Gao,  
371 W., and Li, L.: Development and characterization of a high-performance single-particle aerosol  
372 mass spectrometer (HP-SPAMS), *Atmos. Meas. Tech.*, 17, 1037-1050, 10.5194/amt-17-1037-



- 373 2024, 2024.
- 374 Fergenson, D. P., Pitesky, M. E., Tobias, H. J., Steele, P. T., Czerwiec, G. A., Russell, S. C.,  
375 Lebrilla, C. B., Horn, J. M., Coffee, K. R., Srivastava, A., Pillai, S. P., Shih, M.-T. P., Hall, H. L.,  
376 Ramponi, A. J., Chang, J. T., Langlois, R. G., Estacio, P. L., Hadley, R. T., Frank, M., and Gard,  
377 E. E.: Reagentless Detection and Classification of Individual Bioaerosol Particles in Seconds,  
378 *Analytical Chemistry*, 76, 373-378, 10.1021/ac034467e, 2004.
- 379 Hari, S., McFarland, A. R., and Hassan, Y. A.: CFD Study on the Effects of the Large Particle  
380 Crossing Trajectory Phenomenon on Virtual Impactor Performance, *Aerosol Science and*  
381 *Technology*, 41, 1040-1048, 10.1080/02786820701697549, 2007.
- 382 Hwang, T.-H., Kim, S.-H., Kim, S. H., and Lee, D.: Reducing particle loss in a critical orifice and  
383 an aerodynamic lens for focusing aerosol particles in a wide size range of 30 nm — 10  $\mu$ m,  
384 *Journal of Mechanical Science and Technology*, 29, 317-323, 10.1007/s12206-014-1238-4,  
385 2015.
- 386 Lee, K.-S., Hwang, T.-H., Kim, S.-H., Kim, S. H., and Lee, D.: Numerical Simulations on  
387 Aerodynamic Focusing of Particles in a Wide Size Range of 30 nm–10  $\mu$ m, *Aerosol Science*  
388 *and Technology*, 47, 1001-1008, 10.1080/02786826.2013.808737, 2013.
- 389 Liu, P., Ziemann, P. J., Kittelson, D. B., and McMurry, P. H.: Generating Particle Beams of  
390 Controlled Dimensions and Divergence: II. Experimental Evaluation of Particle Motion in  
391 Aerodynamic Lenses and Nozzle Expansions, *Aerosol Science and Technology*, 22, 314-324,  
392 10.1080/02786829408959749, 1995.
- 393 Liu, P. S. K., Deng, R., Smith, K. A., Williams, L. R., Jayne, J. T., Canagaratna, M. R., Moore, K.,  
394 Onasch, T. B., Worsnop, D. R., and Deshler, T.: Transmission Efficiency of an Aerodynamic  
395 Focusing Lens System: Comparison of Model Calculations and Laboratory Measurements for  
396 the Aerodyne Aerosol Mass Spectrometer, *Aerosol Science and Technology*, 41, 721-733,  
397 10.1080/02786820701422278, 2007.
- 398 Loh, N. D., Hampton, C. Y., Martin, A. V., Starodub, D., Sierra, R. G., Barty, A., Aquila, A.,  
399 Schulz, J., Lomb, L., Steinbrener, J., Shoeman, R. L., Kassemeyer, S., Bostedt, C., Bozek, J.,  
400 Epp, S. W., Erk, B., Hartmann, R., Rolles, D., Rudenko, A., Rudek, B., Foucar, L., Kimmel, N.,  
401 Weidenspointner, G., Hauser, G., Holl, P., Pedersoli, E., Liang, M., Hunter, M. S., Gumprecht,  
402 L., Coppola, N., Wunderer, C., Graafsma, H., Maia, F. R. N. C., Ekeberg, T., Hantke, M.,  
403 Fleckenstein, H., Hirsemann, H., Nass, K., White, T. A., Tobias, H. J., Farquar, G. R., Benner, W.  
404 H., Hau-Riege, S. P., Reich, C., Hartmann, A., Soltau, H., Marchesini, S., Bajt, S., Barthelmeß,  
405 M., Bucksbaum, P., Hodgson, K. O., Strüder, L., Ullrich, J., Frank, M., Schlichting, I., Chapman,  
406 H. N., and Bogan, M. J.: Fractal morphology, imaging and mass spectrometry of single aerosol  
407 particles in flight, *Nature*, 486, 513-517, 10.1038/nature11222, 2012.
- 408 Meinen, J., Khasminkaya, S., Rühl, E., Baumann, W., and Leisner, T.: The TRAPS Apparatus:



- 409 Enhancing Target Density of Nanoparticle Beams in Vacuum for X-ray and Optical  
410 Spectroscopy, *Aerosol Science and Technology*, 44, 316-328, 10.1080/02786821003639692,  
411 2010.
- 412 Murphy, D. M., Cziczo, D. J., Froyd, K. D., Hudson, P. K., Matthew, B. M., Middlebrook, A. M.,  
413 Peltier, R. E., Sullivan, A., Thomson, D. S., and Weber, R. J.: Single-particle mass spectrometry  
414 of tropospheric aerosol particles, *Journal of Geophysical Research: Atmospheres*, 111,  
415 10.1029/2006jd007340, 2006.
- 416 Peck, J., Gonzalez, L. A., Williams, L. R., Xu, W., Croteau, P. L., Timko, M. T., Jayne, J. T.,  
417 Worsnop, D. R., Miake-Lye, R. C., and Smith, K. A.: Development of an aerosol mass  
418 spectrometer lens system for PM<sub>2.5</sub>, *Aerosol Science and Technology*, 50, 781-789,  
419 10.1080/02786826.2016.1190444, 2016.
- 420 Schreiner, J., Schild, U., Voigt, C., and Mauersberger, K.: Focusing of Aerosols into a Particle  
421 Beam at Pressures from 10 to 150 Torr, *Aerosol Science and Technology*, 31, 373-382,  
422 10.1080/027868299304093, 1999.
- 423 Schreiner, J., Voigt, C., Mauersberger, K., McMurry, P., and Ziemann, P.: Aerodynamic Lens  
424 System for Producing Particle Beams at Stratospheric Pressures, *Aerosol Science and  
425 Technology*, 29, 50-56, 10.1080/02786829808965550, 1998.
- 426 Srivastava, A., Pitesky, M. E., Steele, P. T., Tobias, H. J., Fergenson, D. P., Horn, J. M., Russell, S.  
427 C., Czerwiec, G. A., Lebrilla, C. B., Gard, E. E., and Frank, M.: Comprehensive Assignment  
428 of Mass Spectral Signatures from Individual *Bacillus atrophaeus* Spores in Matrix-Free Laser  
429 Desorption/Ionization Bioaerosol Mass Spectrometry, *Analytical Chemistry*, 77, 3315-3323,  
430 10.1021/ac048298p, 2005.
- 431 Tobias, H. J., Pitesky, M. E., Fergenson, D. P., Steele, P. T., Horn, J., Frank, M., and Gard, E. E.:  
432 Following the biochemical and morphological changes of *Bacillus atrophaeus* cells during the  
433 sporulation process using Bioaerosol Mass Spectrometry, *Journal of Microbiological Methods*,  
434 67, 56-63, 10.1016/j.mimet.2006.03.001, 2006.
- 435 Wang, X. and McMurry, P. H.: An experimental study of nanoparticle focusing with aerodynamic  
436 lenses, *International Journal of Mass Spectrometry*, 258, 30-36, 10.1016/j.ijms.2006.06.008,  
437 2006.
- 438 Wang, X., Kruis, F. E., and McMurry, P. H.: Aerodynamic Focusing of Nanoparticles: I.  
439 Guidelines for Designing Aerodynamic Lenses for Nanoparticles, *Aerosol Science and  
440 Technology*, 39, 611-623, 10.1080/02786820500181901, 2005.
- 441 Williams, L. R., Gonzalez, L. A., Peck, J., Trimborn, D., McInnis, J., Farrar, M. R., Moore, K. D.,  
442 Jayne, J. T., Robinson, W. A., Lewis, D. K., Onasch, T. B., Canagaratna, M. R., Trimborn, A.,  
443 Timko, M. T., Magoon, G., Deng, R., Tang, D., de la Rosa Blanco, E., Prévôt, A. S. H., Smith,  
444 K. A., and Worsnop, D. R.: Characterization of an aerodynamic lens for transmitting particles



445 greater than 1 micrometer in diameter into the Aerodyne aerosol mass spectrometer,  
446 Atmospheric Measurement Techniques, 6, 3271-3280, 10.5194/amt-6-3271-2013, 2013.

447 Wu, X., Omenetto, N., and Winefordner, J. D.: Development, Characterization, and Application of  
448 a Versatile Single Particle Detection Apparatus for Time-Integrated and Time-Resolved  
449 Fluorescence Measurements—Part I: Theoretical Considerations, Laser Chemistry, 2009, 1-10,  
450 10.1155/2009/295765, 2009.

451 Zelenyuk, A., Imre, D., Wilson, J., Zhang, Z., Wang, J., and Mueller, K.: Airborne Single Particle  
452 Mass Spectrometers (SPLAT II & miniSPLAT) and New Software for Data Visualization and  
453 Analysis in a Geo-Spatial Context, Journal of the American Society for Mass Spectrometry, 26,  
454 257-270, 10.1007/s13361-014-1043-4, 2015.

455 Zhang, X., Smith, K. A., Worsnop, D. R., Jimenez, J., Jayne, J. T., and Kolb, C. E.: A Numerical  
456 Characterization of Particle Beam Collimation by an Aerodynamic Lens-Nozzle System: Part I.  
457 An Individual Lens or Nozzle, Aerosol Science and Technology, 36, 617-631,  
458 10.1080/02786820252883856, 2002.

459 Zhang, X., Smith, K. A., Worsnop, D. R., Jimenez, J. L., Jayne, J. T., Kolb, C. E., Morris, J., and  
460 Davidovits, P.: Numerical Characterization of Particle Beam Collimation: Part II Integrated  
461 Aerodynamic-Lens-Nozzle System, Aerosol Science and Technology, 38, 619-638,  
462 10.1080/02786820490479833, 2004.

463